Ultrafast diffraction of tightly focused waves with spatiotemporal stabilization

Carlos J. Zapata-Rodríguez

Departamento de Óptica, Universidad de Valencia, Dr. Moliner 50, 46100 Burjassot, Spain
(carlos.zapata@uv.es)

Received April 17, 2008; revised July 2, 2008; accepted July 2, 2008;
posted July 14, 2008 (Doc. ID 95089); published August 15, 2008

Experimental studies of ultrafast beam shaping have come about from the need to compensate diffraction-induced dispersive effects in femtosecond laser beams. From a theoretical point of view, chromatic matching of diffracted spherical waves in the vicinity of the geometrical focus is attained by applying conveniently dispersive boundary conditions in the far-field zone, a subject thoroughly analyzed in the paraxial regime. For applications demanding high spatial resolution, however, high-numerical-aperture microscope objectives may be employed instead and would lead to nonparaxiality of the focal wavefields. These circumstances have motivated our investigation. Concretely we report on prerequisites for spectral invariance extended to wide-angle geometries, which provides stabilization of the spatiotemporal response in the Fourier plane. In this context, general boundary conditions are given in the frame of the Debye representation of wavefields. Features of this sort of dynamic apodization (spatial filtering) leading to perfect achromatization are described in detail.

OCIS codes: 260.1960, 320.7120.

1. INTRODUCTION

When a monochromatic, uniform, paraxial focused wave is observed in the transverse plane containing the geometrical focus, the diffracted pattern traces an Airy disk of magnitude proportional to the wavelength. Such dispersive character at the Fourier plane is associated with a nondispersive truncation of the focused beam, leading to off-axis effects such as spectral anomalies [1–4] and pulse splitting in the form of delayed boundary waves [5]. In addition, if the spherical beam is modulated periodically by means of a diffraction grating or any other rigid device exciting a given spatial frequency, the central point of the light spot moves outward from the axis following a linear dependence upon the wavelength. This radial chromatic aberration is of relevance in material processing [6–9] and multifocal microscopy [10,11], where the spatiotemporal resolution power may be strongly reduced for off-axis foci.

This sort of spatial mismatching encountered in broadband radiation is also widely analyzed both theoretically [12–15] and experimentally [16] in diffraction of ultrafast collimated beams launched over hard-edge apertures. Here we give emphasis to a paper of Heyman and Melamed [17] where, apart of analyzing the space-time evolution of such radiated wavefields, they suggest an "iso-diffracting" scheme providing directivity to the pulsed radiation. A nondispersive spatial distribution of the diffracted field along the direction of propagation is conditioned by maintaining the same collimating distance for all spectral constituents of the field, which is achieved by source shaping in space and time simultaneously [18,19]. Some authors have even extended this idea to propose diffraction-free Bessel beams with isodiffracting behavior [20]. All these cases have in common that the field is dynamically resized at the "aperture" input plane.

Along the same lines, the possibility of generating a pulsed wave with a prescribed performance from a dynamic aperture antenna was addressed by Shaarawi [21,22]. He investigated various illumination schemes of dynamic apertures to generate localized wavefields (X waves and focus wave modes). All are causally launchable from flat apertures characterized by having time-dependent radii. We point out that finite-time dynamic sources are not purely academic exercises but may be synthesized experimentally. Dispersive imaging is a particularly attractive procedure [23–26] exploiting the fine-tunable wavelength response of zone plates.

In this paper we advance in the subject of directional chromatic compensation of diffracted fields based on a controllable spectral mismatch of the source size in the aperture plane. In particular, the achromatization strategy is released over the transverse focal plane of the diffracted spherical wave. We consider focal beams that are free of longitudinal chromatic aberration in order to account for diffraction-driven chromatic compensation exclusively. Thus, we give a general description of nonparaxial focal waves exhibiting an isodiffracting behavior—not along the optical axis but in the Fourier plane—also coined as in-plane isodiffracting (IPID) waves in [24]. From a theoretical point of view, this scheme is of great interest in optical imaging, since point spread functions (also resolving power) would be independent upon wavelength. Assuming that a nondispersive high-numerical-aperture objective lens is in charge of produc-

ing the IPID focused beam, we provide the necessary space-frequency dynamics of the field at the entrance pupil plane.

2. NONDISPERSIVE INTERFERENCE: ISODIFFRACTING WAVES

In this section we establish the role of the angular spectrum dispersion in the spatial patterning of propagating waves, illustrated with the following simple example of interference. Consider two oblique, polychromatic, plane waves of equal strength. The wavevector of each spectral component is denoted by $\mathbf{k}_p$, for $p=\{1,2\}$, being $\|\mathbf{k}_p\|=k$. Here the wavenumber

$$k(\omega)=\frac{\omega n(\omega)}{c}, \tag{1}$$

where ω is the angular frequency, n stands for the index of refraction of the dielectric medium where beam propagation is experienced, and c is the speed of light in vacuum. The interference field is proportional to

$$\exp(i\mathbf{k}_z\mathbf{R})\cos(\mathbf{k}_t\mathbf{R}), \tag{2}$$

where $\mathbf{R}$ is a 3D vector denoting the spatial coordinates of the observation point, and

$$\mathbf{k}_z=\frac{\mathbf{k}_1+\mathbf{k}_2}{2} \tag{3}$$

$$\mathbf{k}_t=\frac{\mathbf{k}_1-\mathbf{k}_2}{2} \tag{4}$$

are perpendicular vectors of modulus $k_z=k\cos\theta$ and $k_t=k\sin\theta$, respectively (shown in Fig. 1.) Along the direction of $\mathbf{k}_z$, each monochromatic component of the wave superposition behaves like an homogeneous wave propagating at a superluminal phase velocity $v_p=c/n\cos\theta$. Contrarily, a standing wave is found in the transverse direction, where k_t gives the spatial frequency of the interference fringes.

In the presently existing broadband problem, we consider a convenient combination of this sort of interfering wave having different frequencies. Commonly, the angle $\theta(\omega)=\alpha$ is conserved under a change of frequency, as schematically shown in Fig. 1(a). In the transverse direction—aimed by $\mathbf{k}_t$—the contrast of the interference fringes is reduced at points increasingly far from the origin due to the dispersive character of the spatial frequency $k_t(\omega)=k(\omega)\sin\alpha$. For temporally coherent sources, this effect leads to the onset of stationary, spatiotemporal localized X waves [27,28].

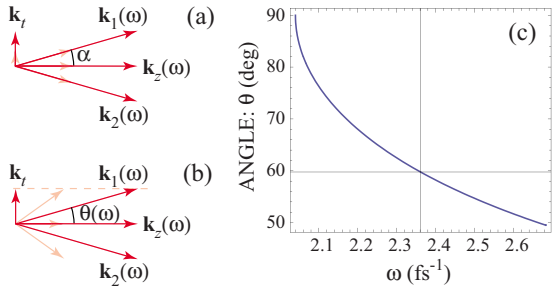

Fig. 1. (Color online) Left column: Schematic representation (a) of 2D X waves and (b) wavefields with transverse isodiffracting behavior. (c) Angular dispersion of a 2D TID wave of $k_t=6.8\ \mu\text{m}^{-1}$ propagating in vacuum.

However, high contrast around not only a central point but also far off-axis may be required. In this sense, transverse isodiffracting (TID) wavefields have the particular property of conserving $\mathbf{k}_t$ for all the spectral components, graphically illustrated in Fig. 1(b), thus guaranteeing the maximum interference contrast in spite of bandwidth. We point out that TID waves are recognized as a 2D version of the so-called pulsed Bessel beams [29–31]. Spectral locking of $\mathbf{k}_t$ is accomplished at the cost of angular dispersion, expressed as

$$\theta(\omega)=\arcsin\left[\frac{k_0}{k(\omega)}\sin\theta_0\right], \tag{5}$$

where the subindex 0 stands for the specific value attained at the frequency ω_0. Moreover, angular dispersion of paraxial waves ($\theta\ll 1$) in vacuum is reduced to $\theta(\omega)=\theta_0\omega_0/\omega$ following a well-known inverse law. Obviously, invariance of $\mathbf{k}_t$ induces a dispersion effect onto the axial wavevector $\mathbf{k}_z$, which may be not dispersed angularly; only its modulus

$$k_z=\sqrt{k^2(\omega)-k_t^2} \tag{6}$$

depends on ω. Particularly, homogeneous (not evanescent) TID wavefunctions are achieved under the constraint $\|\mathbf{k}_t\|\le k(\omega)$, which may bring serious restrictions onto the source bandwidth. In Fig. 1(c) we represent the angular deviation $\theta(\omega)$ of TID waves propagating in vacuum at $k_t=6.8\ \mu\text{m}^{-1}$. We observe that θ reaches a maximum value of 90 deg for a frequency $2.04\ \text{fs}^{-1}$, and it cannot have real values for redder spectral components.

Let us underline some relevant features of the (3+1)D dynamics of the TID pulsed wavefields given above. In the time domain, the wavefunction is described by the integral representation

$$\cos(\mathbf{k}_t\mathbf{r})\int|S(\omega)|\cos[k_z(\omega)z-\omega t+\varphi(\omega)]\mathrm{d}\omega,$$

where $(\mathbf{r},z)=\mathbf{R}$ denotes the transverse ($\mathbf{r}$) and axial (z) coordinates, and S stands for the complex spectral amplitude (of argument φ) evaluated at $\|\mathbf{R}\|=0$. The cut-off frequency ω_c satisfies $k(\omega_c)=k_t$, which gives the low-band boundary where one finds imaginary values of $k_z(\omega)$. In our analysis, we conveniently impose that $S(\omega)=0$ for $\omega\le\omega_c$. In the input plane $z=0$, both $S(\omega)$ and the waveform of the pulse are conserved except for an inversion at negative values of $\cos(\mathbf{k}_t\mathbf{r})$ [32,33]. Similarly, at points of any other transverse plane the TID field possesses the same spectrum (normalized to its maximum value) but distorted from S and, therefore, time evolution is mimetically reproduced over the entire plane. We consider as illustration the following numerical example. We assume a Poisson-type spectrum,

$$S(\omega') = (\omega'\tau_0)^s \exp(-\omega'\tau_0), \tag{7}$$

for $\omega' = \omega - \omega_c \geq 0$ and $S(\omega') = 0$ if $\omega' < 0$. The parameters $\tau_0 = 28$ fs and $s = 8$ provide a pulse form of carrier (mean) frequency $\omega_0 = 2.36$ fs^{-1} and a quasi-Gaussian envelope profile of width $\Delta t = 9.6$ fs (at which the envelope intensity drops to $1/e$). Pulse propagation is evaluated in vacuum for a TID wave of invariant $k_t = 6.8$ μm^{-1}, for which a cutoff frequency $\omega_c = 2.04$ fs^{-1} is found. For comparison, we additionally consider a 2D X wave such that, for the carrier frequency, the transverse wavevector coincides with that of the TID field ($k_0 \sin\alpha = k_t$) giving $\alpha = 59.8$ deg. In Fig. 2 we plot the amplitude $|E|$ of (a) the X wave and (b) the TID wave in the meridian plane $y = 0$ for the instant $t = 0$; note that $\mathbf{k}_t$ of both pulsed waves is considered to have a vector component of modulus zero along the y axis. We evidence that spatial localization of the X wave is observed perpendicularly to the constituents $\mathbf{k}_1$ and $\mathbf{k}_2$, respectively, in planes tilted at angles $\pm(\pi/2 - \alpha)$ from $x = 0$. However, an optimum contrast of the interference fringes is produced in transverse planes for the TID wave, showing a high intensity around $z = 0$ at $t = 0$.

To conclude this section, let us extend our analysis to account for more complex beams consisting of combinations of broadband TID beams, each one with a characteristic $\mathbf{k}_t$ but all having the same amplitude spectrum $S(\omega)$ at a given transverse plane; for instance at $z = 0$. In this particular plane, the diffraction pattern of the composite wavefield is invariant—except maybe for a constant amplitude—under a change of frequency. This case is commonly encountered in diffraction of polychromatic light passing through an aperture. In this context, Heyman *et al.* [17] coined the term iso-width aperture to refer to the exit pupil of optical systems launching this sort of radiation pattern. In transverse planes where $z \neq 0$, the complex spectral modifier $\exp[ik_z(\omega)z]$ alters differently the spectrum of each TID component, since k_z is itself different. Additionally, a noncoincident spatial frequency of the interference fringes associated with each TID component leads to a distinct modification of the spectrum at different points in a given transverse plane. As a consequence, a spatial dispersion is induced in out-of-plane wavefields; such an effect is widely reported in the literature for bell-shaped optical waves. For instance, a Gaussian beam of width $a(z)$ independent of the frequency at $z = 0$ propagates in vacuum in such a way that

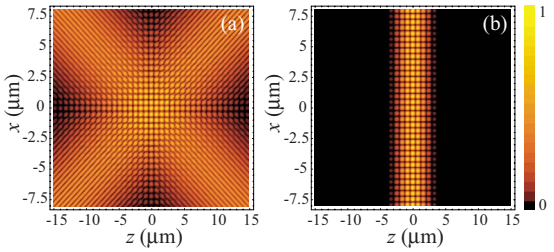

Fig. 2. (Color online) Instantaneous amplitude $|E(x,z)|$ of (a) a 2D X wave and (b) a TID wavefield, where the carrier frequency $\omega_0 = 2.36$ fs^{-1}, the pulse width is 9.6 fs, and the angular deviation $\theta(\omega_0) = 59.8$ deg.

$$a(z) = \sqrt{a^2(0) + \frac{4c^2z^2}{a^2(0)\omega^2}} \tag{8}$$

varies spectrally for $z \neq 0$. Therefore, such a combination does not represent a new TID wave and, as much, we may speak of beams with isodiffracting behavior in the privileged plane $z = 0$, or simply IPID beams.

3. FOCALIZATION WITH RIGID APERTURING AND FILTERING

Before analyzing under which conditions chromatic invariance of focal wavefields may be achieved, in this section we give relevant aspects of broadband wave focalization with particular emphasis on diffraction-induced off-axis effects. Let us describe a general focused field in terms of the Debye representation

$$\tilde{E}(\mathbf{R},\omega) = \frac{-ik(\omega)}{2\pi} \int \tilde{E}_0(\Omega,\omega)\exp[i\mathbf{k}(\omega)\mathbf{R}]\mathrm{d}\Omega. \tag{9}$$

The integral representation of the field as formulated here is appropriate in our theoretical analysis, since it considers a superposition of plane waves denoting $\tilde{E}_0$ the strength of its constituents. In Eq. (9) Ω stands for a solid angle and therefore

$$\mathrm{d}\Omega = \sin\theta \mathrm{d}\theta \mathrm{d}\varphi, \tag{10}$$

where θ is the polar angle from the z axis with $0 \leq \theta \leq \pi/2$, as shown in Fig. 3, and φ is the azimuthal angle in the transverse $\mathbf{r}$ plane with $0 \leq \varphi < 2\pi$.

Under the Debye approximation, if a uniform, broadband, plane wave is focused by an achromatic objective lens, the focal wavefield is free of angular dispersion [23,34]. This property remains when the incident plane wave is additionally apertured by hard-edge apodizing screens or, in general, modulated by any rigid (nondispersive) diffracting element if its characteristic spatial spectrum has a band distribution that is sufficiently low. These sort of focal wave are coined as iso-angular-spectrum (IAS) beams elsewhere [24]. In this particular case, a factorization of the form

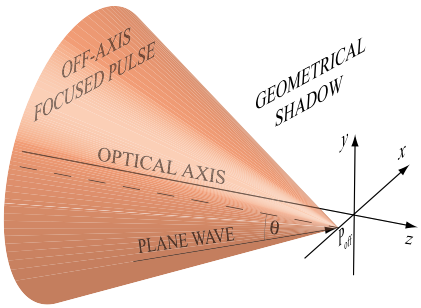

Fig. 3. (Color online) Schematic depiction of an off-axis focused wave. Induced by diffraction, plane-wave constituents are phase-matched at P_{off}, a point placed at the transverse $\mathbf{r} = (x,y)$ plane. Considering the function $F(\mathbf{q})$ of Eq. (21), a point P_{off} would be found at a distance $\Delta/k_0 q_m$ from the origin, together with another one symmetrically arranged along the x axis.

$$\tilde{E}_0(\Omega,\omega) = S(\omega)P(\Omega) \tag{11}$$

is allowed, where S represents the amplitude spectrum of the incident beam and P gives the forward-propagating field evaluated over the convergent spherical wavefront beyond the focal region,

$$\tilde{E}(\mathbf{R},\omega) \overset{kR\gg 1}{\rightarrow} S(\omega)P(\Omega)\frac{\exp(-ikR)}{R}\ (z<0), \tag{12}$$

which is coincident for each spectral component. For convenience we tentatively write

$$P(\Omega) = iF(\mathbf{k}_t/k)\cos\theta, \tag{13}$$

where

$$\cos\theta = \frac{k_z}{k} \tag{14}$$

serves the function of an obliquity factor, and

$$\mathbf{k}_t = (k_x,k_y) = k\sin\theta(\cos\varphi,\sin\varphi) \tag{15}$$

gives the relationship between the transverse wavevector $\mathbf{k}_t$ and the angular coordinates θ and φ. Here, we have made use of the (spatial) dispersion equation $k^2=\mathbf{k}_t\mathbf{k}_t+k_z^2$. Achromaticity of the azimuthal and the polar angles from the plane-wave constituents of the focused field makes our choice in Eq. (13) fully compatible with the independence of the function P upon ω.

For convenience, the Debye integral representation of the focused wave given in Eq. (9) is expressed in the 2D domain $\mathbf{k}_t$. After substitution of Eqs. (11) and (13) into Eq. (9) and using

$$\mathrm{d}\Omega = \mathrm{d}\mathbf{k}_t/kk_z, \tag{16}$$

we have that the focal field is evaluated by

$$\tilde{E}(\mathbf{R},\omega) = \frac{S(\omega)}{2\pi k(\omega)}\int F(\mathbf{k}_t/k)\cos(\mathbf{k}_t\mathbf{r})\exp(ik_z z)\mathrm{d}\mathbf{k}_t, \tag{17}$$

where $k_z=\sqrt{k^2-\mathbf{k}_t\mathbf{k}_t}$. In Eq. (17) we have assumed that F is an even function, $F(-\mathbf{k}_t/k)=F(\mathbf{k}_t/k)$, so that the above-given integral is straightforwardly interpreted as a continuous superposition of interference waves of the kind shown in Eq. (2), providing $|F|^2$ the spectral intensity with characteristic $\mathbf{k}_t$. As analyzed in Section 2, we expect that the dispersive character of $k(\omega)$ is extended over $\mathbf{k}_t$, which decreases the visibility of the interference fringes for each transverse spatial frequency and, therefore, reduces the contrast of the composite diffraction pattern in the transverse direction. As a consequence, a strong spatiotemporal spreading of the focused pulse may be anticipated.

In our study we are particularly concerned with the spatial-temporal evolution of the spherical wave in its focal plane. Therefore, we consider the diffracted field in Eq. (17) at $z=0$, giving

$$\tilde{E}(\mathbf{r},\omega) = k(\omega)S(\omega)G[k(\omega)\mathbf{r}], \tag{18}$$

where

$$G(\boldsymbol{\rho}) = (2\pi)^{-1}\int F(\mathbf{q})\exp(i\mathbf{q}\boldsymbol{\rho})\mathrm{d}\mathbf{q} \tag{19}$$

is the 2D Fourier transform of F. Except for an external factor, G provides the diffraction pattern for every spectral constituent of the field, which is affected by a frequency-dependent lateral magnification $k^{-1}(\omega)$. Obviously, the magnification of the wavefield is inversely proportional to ω in vacuum as, for instance, in the way it is found in the Airy disk when F represents a binary circular function. We point out that, in a general case, not only is the diffracted field spatially dispersed in the focal plane, but—also as a consequence—the amplitude spectrum changes locally; this is a feature also observed in out-of-focus planes [2]. At points sufficiently close to the optical axis where $G(k\mathbf{r})\rightarrow G(\mathbf{0})$, the wave form is proportional to the real part of

$$\int k(\omega)S(\omega)\exp(-i\omega t)\mathrm{d}\omega, \tag{20}$$

neglecting the carrier phase [29] $\exp\{i\arg[G(\mathbf{0})]\}$. In nondispersive media, the spectrum is proportional to $\omega S(\omega)$ demonstraating a well-known time-derivative behavior [35]. On the contrary, G varies rapidly at points sufficiently far from the geometrical focus, which provokes stretching—and ultimately splitting—of the pulse [5].

To illustrate the dispersion-induced decrease of spatiotemporal resolution in the focal plane of an IAS wave, we examine the function

$$F(\mathbf{q}) = \cos(\Delta q_x/q_m)\mathrm{circ}(q/q_m), \tag{21}$$

where $\mathbf{q}=(q_x,q_y)$ of modulus

$$q = \sqrt{q_x^2+q_y^2},$$

q_m and Δ are real positive constants, and $\mathrm{circ}(\beta)=1$ if $\beta\leq 1$ [otherwise $\mathrm{circ}(\beta)=0$]. This particular F simultaneously considers diffraction onto a holographic-type grating, which produces an equienergetic beam splitting, together with beam aperturing of the collecting objective lens. In this case, $q_m=\sin\alpha$ is interpreted as the numerical aperture—in vacuum—of the focal wave. We perform the 2D Fourier transform of Eq. (19) and obtain

$$G(\boldsymbol{\rho}) = \frac{G_D(\boldsymbol{\rho}+\boldsymbol{\rho}_0)+G_D(\boldsymbol{\rho}-\boldsymbol{\rho}_0)}{2}, \tag{22}$$

where $\boldsymbol{\rho}_0=(\Delta/q_m,0)$ and

$$G_D(\boldsymbol{\rho}) = \frac{q_m\mathrm{J}_1(q_m\rho)}{\rho}. \tag{23}$$

At ω_0, phase matching of plane-wave constituents is produced at two points found at a distance Δ/k_0q_m from the origin of the $\mathbf{r}$ plane (see Fig. 3). Obviously, spatial dispersion is better explored by selecting a grating of appropriate low frequency; if $\Delta=1.22\pi$, the distance between the diffraction orders is twice the resolution limit following the Rayleigh criterion.

Again, we performed numerical simulations with an amplitude spectrum of the Poisson type and with parameters as those used in Fig. 2. Particularly, focal waves are

imposed to have an angular aperture $\alpha=59.8$ deg, which is equivalent to imposing that a maximum value of $k_t=6.8\ \mu\text{m}^{-1}$—ignoring the cos modulation—is reached at $\omega_0=2.36\ \text{fs}^{-1}$. In Fig. 4 we plot the temporal behavior of the focal field $|E|$ along $y=0$. In Figs. 4(a) the geometrical focal point is surrounded at a short distance by the diffraction-induced focal spots and, as a consequence, the dispersion effects are negligible. By increasing either the spatial frequency of the grating or the number of diffraction orders, spots surge separately from the geometrical focal point where the dispersion effects are enhanced. To gain a deeper insight into the spatiotemporal features of off-axis focusing, we conveniently employ the function

$$F_{\text{off}}(\mathbf{q}) = \exp(i\mu q_x/q_m)F(\mathbf{q}), \tag{24}$$

which accounts for a frequency increment of the spatial modulation, thus producing a steering of the launched wave outward of the optical axis. The 2D Fourier transform of F_{off} is

$$G_{\text{off}}(\boldsymbol{\rho}) = G(\boldsymbol{\rho} - \boldsymbol{\rho}_{\text{off}}), \tag{25}$$

with $\boldsymbol{\rho}_{\text{off}}=(-\mu/q_m,0)$. Therefore, F_{off} contemplates a lateral shift of the pair of diffraction spots in terms of the parameter μ. In Figs. 4(b)–4(d) we observe that the pulse elongates and the focal spots become spatially indistinguishable for increasing μ. We point out that the maximum off-axis shift $-\mu/k_0q_m=-11.3\ \mu\text{m}$ is attained at $\mu=20\Delta$ in the plot).

4. MAXIMUM VISIBILITY OF FOURIER PATTERNS: IPID FOCAL WAVES

Compensation of spatiotemporal dispersion effects associated with broadband beam focalization may be carried out in the focal plane by spherical waves of the IPID type. In Section 2 we established that IPID beams have a characteristic plane wherein the diffracted field—here $\tilde{E}(\mathbf{r},\omega)$ at $z=0$—may be factorized into two functions: a first function with spatial independence and the other one being spectrally invariant. In the focal plane, the isodiffracting condition explicitly given ahead in Eq. (27) is accomplished if the input field of the Debye integral representation may be written as

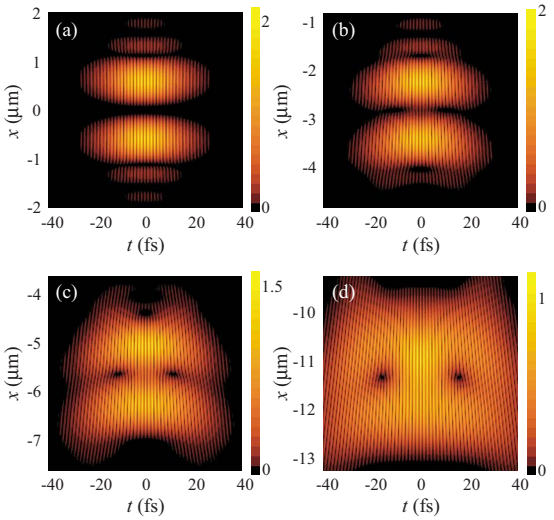

Fig. 4. (Color online) Temporal dynamics of $|E|$ in the focal plane of IAS focal fields with off-axis parameter: (a) $\mu=0$, (b) $\mu=5\Delta$, (c) $\mu=10\Delta$, and (d) $\mu=20\Delta$. Chromatic phase mismatching inducing spatio-temporal stretching (and subsequent attenuation) of the field grows as focalization is produced at points increasingly far from the optical axis.

$$\tilde{E}_0(\Omega,\omega) = iS(\omega)F(\mathbf{k}_t/k_0)\frac{k_z(\omega)}{k_0}. \tag{26}$$

We point out that this equation constitutes itself a boundary condition of the wavefield. Therefore, $\tilde{E}_0$ is modulated by the time-domain spectrum S, the space-domain spectrum F, and the obliquity factor k_z/k_0. Specifically, the spectrum of the beam launched over the focusing system does not necessarily correspond to the function $S(\omega)$, a point discussed in detail in Section 5. Furthermore, the strength of the function F is maintained if the transverse wavevector $\mathbf{k}_t$ is conserved, leading to a given angular dispersion of the plane-wave constituents of the Debye integral. Additionally, the obliquity factor considered here is arbitrary, since the IPID condition is generally attained when such a term is multiplied by a given spatially independent function, for instance a power of $k(\omega)/k_0$.

To determine the focal field in $z=0$ we introduce Eq. (26) into Eq. (9) and we obtain

$$\tilde{E}(\mathbf{r},\omega) = k_0S(\omega)G(k_0\mathbf{r}), \tag{27}$$

where Eqs. (16) and (19) have been employed. Focal fields figured by the function G are invariant under a change of frequency—apart from the factor S—and, as a consequence, spectra at points of the focal plane are proportional to the input spectrum $S(\omega)$. In the time domain, such a conservation of the spectrum leads to an invariance of the pulse form. Importantly, if the spectrum S is a real and positive function, a bandwidth-limited pulse dynamic is observed simultaneously at every point of the focal plane.

To illustrate the spatiotemporal behavior of these IPID focal waves, we again employ the function $F(\mathbf{q})$ given in Eq. (21). The 2D Fourier transform G is also the Airy-disk doublet of Eqs. (22) and (23). In the numerical simulation shown in Fig. 5, the (normalized) spatial frequency of the periodic modulation is $\Delta=1.22\pi$, $k_t=6.8\ \mu\text{m}^{-1}$ is the maximum value of the transverse wavenumber associated with a single unshifted focal beam, and the input spectrum is of the Poisson type as employed in Figs. 2–4. Comparatively, Fig. 5 shows a temporal dynamic resembling that of Fig. 4(a), which corresponds to an IAS multifocal beam. As previously discussed, focalization of these IAS waves is being performed sufficiently close to the optical axis that dispersive effects may be neglected. For this reason, we consider again large displacements of the focal doublet far off the geometrical focus, addressed by means of the function F_{off} given in Eq. (24). When F_{off} substitutes the spatial spectrum F of the IPID focal wave, the temporal evolution of the pulse may be represented graphically by the same Fig. 5 if we replace the spatial coordinate x shown in the ordinate of the plot by

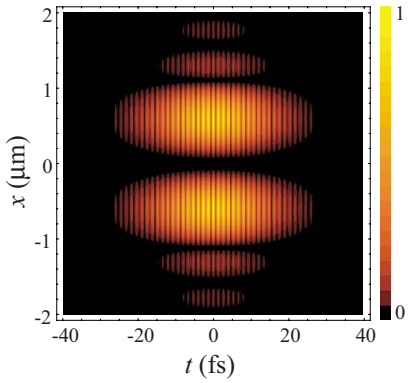

Fig. 5. (Color online) Time evolution of the IPID field $|E|$ along the grating pitch direction ($y=0$) of the focal plane.

$$x \to x + \frac{\mu}{k_0 q_m}. \tag{28}$$

As expected, the spatiotemporal resolution of the multifocal beam remains invariant over any target area in the focal plane.

Let us conclude our analysis with the pulse dynamics in out-of-focus planes. We compare behaviors of IAS and IPID defocused waves to estimate in which measure diffraction-induced dispersion may strike the resolution power along the propagation direction; observation at a given point in time may provide an "instantaneous" depth of focus. Figure 6 explores the field $|E|$ in the meridian plane $y=0$ of the focal volume at $t=0$. In the case of IPID waves—seen in Fig. 6(a) at $\mu=20\Delta$—the instantaneous depth of field remains invariant with respect to the on-axis case $\mu=0$, demonstrating optimum 3D spatial resolution. Contrarily, the IAS wave shown in Fig. 6(b) is not only unable to resolve the diffraction doublet but exhibits a substantially increased depth of field. In this respect we point out that, except for IPID waves, the reduction of the axial resolution is intensified as moving further from the optical axis, so that the instantaneous depth of field generally becomes a shift-variant feature of ultrashort focal waves.

5. DYNAMIC ENTRANCE PUPIL

Focal fields with an IPID response demonstrate that diffraction-induced dispersion may be compensated. Thus we have a capacity for rendering bandwidth-length pulses simultaneously in the focal plane. With this goal the

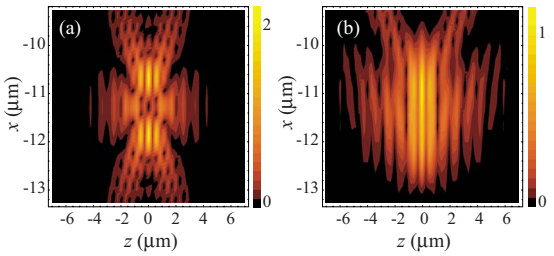

Fig. 6. (Color online) Axial response of the instantaneous field $|E|$ at the local time $t=0$ for (a) an IPID wave and (b) an IAS focused field, both at $\mu=20\Delta$. The IAS wave undergoes a considerable increment of the depth of field.

spherical wave is conveniently modulated beyond the focal region in the form given in Eq. (26). Experimentally, such a modulation is commonly imprinted by optical elements placed in front of a microscope objective being in charge of the beam focusing. Therefore, synthesis of IPID focused fields requires a description of the pulsed wave at an input plane (entrance pupil plane for convenience) as it impinges onto the focusing lens system.

For simplicity, we consider a collimated (and modulated) beam launched over an infinity-corrected objective lens. The diffracted field at the entrance pupil plane may be written as

$$\tilde{E}_{in}(\mathbf{r}_i,\omega) = S_{in}(\omega) T(\omega,\mathbf{r}_i), \tag{29}$$

where the spectrum S_{in} combines spatially independent terms of the input field and, for convenience, we may impose $T(\omega,\mathbf{0})=T(\omega_0,\mathbf{0})$. The pattern T accounts for beam filtering driven by diffracting optical elements—such as spatial light modulators and gratings—and aperturing caused by the diffraction-limited objective lens. In particular, the spectral dependence of T may be induced by free-space propagation [24], zone-plate-assisted imaging [26], and any other dispersive process. A magnified version of $\tilde{E}_{in}$ is reproduced at the exit pupil plane of the lens system, where the focusing elements additionally produce a convergent spherical wavefront. In the way it is described in Eq. (12), we may write the field at the exit pupil plane as

$$\tilde{E}_{out}(\mathbf{R},\omega) = \tilde{E}_0(\Omega,\omega)\frac{\exp(-ikR)}{R}, \tag{30}$$

where R is the distance measured from the geometrical focus. Lossless focalization allows conservation of wave energy flux at the entrance and exit pupil planes providing the following ligature [36]:

$$\int |S_{in}(\omega)|^2 |T(\omega,\mathbf{r}_i)|^2 \mathrm{d}\mathbf{r}_i = \int |\tilde{E}_0(\Omega,\omega)|^2 \mathrm{d}\Omega. \tag{31}$$

By using Eqs. (16) and (26), the energy conservation law and the IPID condition are simultaneously fulfilled if

$$T(\omega,\mathbf{r}_i) = i\frac{S(\omega)}{S_{in}(\omega)}\sqrt{\frac{Jk_z}{kk_0^2}}F(\mathbf{k}_t/k_0), \tag{32}$$

where $\mathbf{k}_t$ explicitly depends upon the plane coordinate $\mathbf{r}_i$ and J is the determinant of the Jacobian matrix

$$\frac{\partial(\mathbf{k}_t)}{\partial(\mathbf{r}_i)} = \begin{bmatrix} \frac{\partial k_x}{\partial x_i} & \frac{\partial k_x}{\partial y_i} \\ \frac{\partial k_y}{\partial x_i} & \frac{\partial k_y}{\partial y_i} \end{bmatrix}. \tag{33}$$

The relationship between $\mathbf{r}_i$ and $\mathbf{k}_t$ is brought by the specific characteristics of the focusing lens system, which is commonly computed from ray tracing procedures. Concisely, a ray is first considered propagating parallel to the optical axis impinging upon a point at coordinates $\mathbf{r}_i$ in the entrance pupil plane. At the exit plane, such a ray has bent its trajectory toward the focus pointing in the direction of the wavevector $\mathbf{k}$, which is employed in the Debye

representation (9) and has transverse coordinates $\mathbf{k}_t$. In axisymmetric optical systems, $\mathbf{r}_i$ and $\mathbf{k}_t$ are contained in the same meridian plane and, as a consequence, they are parallel vectors satisfying $\mathbf{r}_i\mathbf{k}_t = \pm r_i k_t$. Accordingly, $\mathbf{r}_i$ and $\mathbf{k}_t$ are suitably expressed in cylindrical coordinates so that the Jacobian determinant is reduced to

$$J = \frac{\partial(k_t^2)}{\partial(r_i^2)}. \tag{34}$$

Interestingly, $J \propto k^2$ for nondispersive focusing elements—diffractive elements such as zone plates have a characteristic J that is invariant upon ω—and we may write

$$T(\omega,\mathbf{r}_i) = i\frac{S(\omega)k(\omega)}{S_{in}(\omega)k_0}\sqrt{\frac{J_0\cos\theta}{k_0^2}}F(\mathbf{k}_t/k_0), \tag{35}$$

where J_0 is the Jacobian determinant at the carrier frequency. The first term depends exclusively upon the frequency, providing how the input spectrum S_{in} is transformed into

$$S(\omega) = -i\gamma\frac{k_0}{k(\omega)}S_{in}(\omega) \tag{36}$$

in the focal plane, where $\gamma = k_0 T(\omega_0,\mathbf{0})/\sqrt{J_0}F(\mathbf{0})$. These spectral transformations have been analyzed in [24] in free-space paraxial propagation; when the medium is nondispersive, $k \propto \omega$ and we may observe an antiderivative (integral) time response. Here we have included a $\pi/2$-shift of the carrier-envelope phase for convenience.

To illustrate our analysis, let us consider a nondispersive infinity-corrected objective lens system that fulfills the sine condition. From its characteristic ray projection function [37], $r_i/f = \sin\theta$, we obtain

$$\frac{r_i}{f} = \frac{k_t}{k}, \tag{37}$$

where f is the focal distance of the lens system. Since $\mathbf{r}_i$ and $\mathbf{k}_t$ are antiparallel for $f>0$, we may provide a vectorial form of Eq. (37) giving

$$\mathbf{k}_t = -\frac{k}{f}\mathbf{r}_i. \tag{38}$$

In this case, the Jacobian determinant is $J = k^2/f^2$. Finally, the input pattern T capable of generating an IPID response in the focal plane of the objective lens may be expressed as

$$T(\omega,\mathbf{r}_i) = \left(1 - \frac{r_i^2}{f^2}\right)^{1/4} F(-\mathbf{r}_i/fM), \tag{39}$$

where an irrelevant factor γ/f has been omitted and where $M(\omega) = k_0/k(\omega)$ stands for a magnification parameter. The spectrally invariant fourth root is commonly associated with a rigid apodization, which may be performed by purely absorbing screens conveniently placed at the entrance pupil plane. On the other hand, the wavefunction F requires rescaling if the frequency is different than ω_0. As a consequence, a given modulation of the input beam should be dynamically patterned at the input plane of the objective lens following a geometric mapping that is governed by the dispersive magnification M.

We point out that rigid apodization surges in high-numerical-aperture geometries imposed by the angular dependence of the term Jk_z. Obviously, we may get rid of such a rigid apodization if

$$Jk_z = \frac{k^3}{f^2}. \tag{40}$$

Note that such a constraint strictly holds within the paraxial approximation ($k_z \to k$). When we solve the previous differential equation, conveniently expanded as

$$\frac{\partial(k_t^2)}{\partial(r_i^2)}\sqrt{k^2 - k_t^2} = \frac{k^3}{f^2}, \tag{41}$$

we obtain a solution leading to the ray projection function

$$\frac{r_i}{f} = \sqrt{\frac{2}{3}}\sqrt{1 - \left[1 - \left(\frac{k_t}{k}\right)^2\right]^{3/2}} = \sqrt{\frac{2}{3}}\sqrt{1 - \cos^3\theta}. \tag{42}$$

Under the present conditions of focalization, the IPID behavior is achieved if the wavefield at the pupil plane responds exclusively to the appropriate dispersive mapping of F.

To conclude, we reexamine the dynamic apodization of IPID focal waves in the paraxial regime, which has been investigated elsewhere [23,24]. Specifically, the ray projection function approaches θ so that Eq. (37) holds once again. In a low-numerical-aperture focalization $r_i \ll |f|$ and Eq. (39), providing the amplitude distribution at the entrance pupil plane reduces to

$$T(\omega,\mathbf{r}_i) = F(-\mathbf{r}_i/fM). \tag{43}$$

In this respect, some approaches have been proposed in the literature in order to achieve the required mapping in free-space propagation. Concretely, [26] exploits the less-stringent constraint

$$\frac{\mathrm{d}(\omega M)}{\mathrm{d}\omega} = 0, \tag{44}$$

imposed at $\omega = \omega_0$. In nondispersive media, Eq. (44) leaves $k(\omega)M(\omega)$ spectrally stationary in the vicinity of the carrier frequency. This achromatic (first-order) solution gives an appropriate IPID response at the focal plane for pulses of narrow and moderate bandwidths.

6. CONCLUSIONS

Spatiotemporal resolution in the Fourier plane of ultrashort focused beams is analyzed under boundary conditions capable to alter differently the "visibility" of such polychromatic diffracted fields. When the visibility is maximum we speak of an in-plane isodiffracting (IPID) behavior of the Fourier pattern, preventing from its common centrosymmetric spectrally dependent magnification that ultimately is responsible for diffraction-induced chro-

matic aberrations. In this case, ultrafast beam shaping is performed to provide a diffracted field fully free of dispersion effects.

In particular, diffraction-driven steering inducing off-axis focalization associated with an IPID spherical wave is produced not only with compensated angular dispersion but also conserves the extent of the diffraction pattern corresponding to each spectral constituent of the field. In the frame of this model, the limit of resolution following, for instance, the Rayleigh criterion is independent of the wavelength. A convenient interpretation is given in terms of dynamic apodization. Aperturing of a focused IPID wavefield is spectrally dispersed, and so the angular spectrum, in the sense that numerical aperture conveniently changes at different frequencies to keep the focal spot size unaltered.

At the entrance pupil plane, a given rigid (nondispersive) apodization may be additionally imposed in order to meet isodiffracting conditions in the focal plane. Such rigid apodization varies upon the ray projection function associated with the focusing element. In fact, we give a particular projection function for which rigid apodization may be ignored. Importantly, we have shown how the input waveform is transformed as the beam is delivered to the focal plane. Concerning rigorously nondispersive lens systems, we have demonstrated that an antiderivative law is obeyed under IPID boundary conditions. Description of experimental procedures to attain such dynamic spatial filtering is out of the scope of this manuscript; nevertheless, we give a list of references reporting on this question.

ACKNOWLEDGMENTS

This research was funded by the Generalitat Valenciana under project GV/2007/043.

REFERENCES

1. G. Gbur, T. D. Visser, and E. Wolf, "Anomalous behavior of spectra near phase singularities of focused waves," Phys. Rev. Lett. **88**, 013901 (2002).
2. C. J. Zapata-Rodríguez and J. A. Monsoriu, "Spectral anomalies in focused waves of different Fresnel numbers," J. Opt. Soc. Am. A **21**, 2418–2423 (2004).
3. C. J. Zapata-Rodríguez, "Analytical characterization of spectral anomalies in polychromatic apertured beams," Opt. Commun. **257**, 9–15 (2006).
4. C. J. Zapata-Rodríguez, "Spectral anomalies in supercontinuum focused waves," Opt. Commun. **263**, 131–134 (2006).
5. Z. L. Horváth and Z. Bor, "Diffraction of short pulses with boundary diffraction wave theory," Phys. Rev. E **63**, 026601 (2001).
6. B. K. A. Ngoi, K. Venkatakrishnan, B. Tan, P. Stanley, and L. E. N. Lim, "Angular dispersion compensation for acousto-optic devices used for ultrashort-pulsed laser micromachining," Opt. Express **9**, 200–206 (2001).
7. J. Amako, K. Nagasaka, and N. Kazuhiro, "Chromatic-distorsion compensation in splitting and focusing of femtosecond pulses by use of a pair of diffractive optical elements," Opt. Lett. **27**, 969–971 (2002).
8. S. Q. Zeng, X. Lv, C. Zhan, W. R. Chen, W. H. Xiong, Q. Luo, and S. L. Jacques, "Simultaneous compensation of spatial and temporal dispersion of acousto-optical deflectors for two-dimensional scanning with a single prism," Opt. Lett. **31**, 1091–1093 (2006).
9. G. Mínguez-Vega, J. Lancis, J. Caraquitena, V. Torres-Company, and P. Andrés, "High spatiotemporal resolution in multifocal processing with femtosecond laser pulses," Opt. Lett. **31**, 2631–2633 (2006).
10. L. Sacconi, E. Froner, R. Antolini, M. R. Taghizadeh, A. Choudhury, and F. S. Pavone, "Multiphoton multifocal microscopy exploiting a diffractive optical element," Opt. Lett. **28**, 1918–1920 (2003).
11. S. P. Veetil, H. Schimmel, and F. Wyrowski, "Simulation of multibeam imaging in three-dimensional space and time with a diffractive optical element illuminated with a femtosecond pulse," J. Opt. Soc. Am. B **24**, 2580–2583 (2007).
12. M. Gu and X. S. Gan, "Fresnel diffraction by circular and serrated apertures illuminated with an ultrashort pulsed-laser beam," J. Opt. Soc. Am. A **13**, 771–778 (1996).
13. Z. Jiang, R. Jacquemin, and W. Eberhardt, "Time dependence of Fresnel diffraction of ultrashort laser pulses by a circular aperture," Appl. Opt. **36**, 4358–4361 (1997).
14. M. Lefrancois and S. Pereira, "Time evolution of the diffraction pattern of an ultrashort laser pulse," Opt. Express **11**, 1114–1122 (2003).
15. C. J. Zapata-Rodríguez, "Temporal effects in ultrashort pulsed beams focused by planar diffracting elements," J. Opt. Soc. Am. A **23**, 2335–2341 (2006).
16. G. Li, C. Zhou, and E. Dai, "Splitting of femtosecond laser pulses by using a Dammann grating and compensation gratings," J. Opt. Soc. Am. A **22**, 767–772 (2005).
17. E. Heyman and T. Melamed, "Certain consideration in aperture synthesis for ultra wideband/short-pulsed fields," IEEE Trans. Antennas Propag. **AP-42**, 518–525 (1994).
18. M. A. Porras, "Ultrashort pulsed Gaussian light beams," Phys. Rev. E **58**, 1086–1093 (1998).
19. S. Feng and H. G. Winful, "Spatiotemporal structure of isodiffracting ultrashort electromagnetic pulses," Phys. Rev. E **61**, 862–873 (2000).
20. C. J. R. Sheppard, "Generalized Bessel pulse beams," J. Opt. Soc. Am. A **19**, 2218–2222 (2002).
21. A. M. Shaarawi, S. M. Sedky, R. W. Ziolkowski, and I. M. Besieris, "The spatial distribution of the illumination of dynamic apertures and its effect on the decay rate of the radiated localized pulses," J. Phys. A: Math. Gen. **29**, 5157–5179 (1996).
22. A. M. Shaarawi, "Comparison of two localized wave fields generated from dynamic apertures," J. Opt. Soc. Am. A **14**, 1804–1816 (1997).
23. C. J. Zapata-Rodríguez, "Debye representation of dispersive focused waves," J. Opt. Soc. Am. A **24**, 675–686 (2007).
24. C. J. Zapata-Rodríguez, P. Andrés, G. Mínguez-Vega, J. Lancis, and J. A. Monsoriu, "Broadband focused waves with compensated spatial dispersion: transverse versus axial balance," Opt. Lett. **32**, 853–855 (2007).
25. C. J. Zapata-Rodríguez and M. T. Caballero, "Isotropic compensation of diffraction-driven angular dispersion," Opt. Lett. **32**, 2472–2474 (2007).
26. C. J. Zapata-Rodríguez and M. T. Caballero, "Ultrafast beam shaping with high-numerical-aperture microscope objectives," Opt. Express **15**, 308–313 (2007).
27. S. V. Kukhlevsky, G. Nyitray, and V. L. Kantsyrev, "Fields of optical waveguides as waves in free space," Phys. Rev. E **64**, 026603 (2001).
28. M. A. Porras, G. Valiulis, and P. D. Trapani, "Unified description of Bessel X waves with cone dispersion and tilted pulses," Phys. Rev. E **68**, 016613 (2003).
29. M. A. Porras, "Diffraction effects in few-cycle optical pulses," Phys. Rev. E **65**, 026606 (2002).
30. G. Nyitray and S. V. Kukhlevsky, "Distortion-free tight confinement and step-like decay of fs pulses in free space," http://arxiv.org/abs/physics/0310057v1.
31. G. Nyitray, V. Mathew, and S. V. Kukhlevsky, "Generation and interference collapse of distortion-less fs pulses in free space by Fresnel sources," Opt. Commun. **281**, 1082–1086 (2008).
32. S. V. Kukhlevsky and G. Nyitray, "Correlation between

spatial and temporal uncertainties of a wave packet," Opt. Commun. **209**, 377–382 (2002).
33. S. V. Kukhlevsky, "Diffraction-free subwavelength-beam optics on a nanometer scale," in *Localized Waves*, H. E. Hernández-Figueroa, M. Zamboni-Rached, and E. Recami, eds. (Wiley, 2008) pp. 273–297.
34. E. Wolf and Y. Li, "Conditions for the validity of the Debye integral representation of focused fields," Opt. Commun. **39**, 205–210 (1981).
35. A. E. Kaplan, "Diffraction-induced transformation of near-cycle and subcycle pulses," J. Opt. Soc. Am. B **15**, 951–956 (1998).
36. M. Gu, *Advanced Optical Imaging Theory* (Springer, 2000).
37. C. J. R. Sheppard and M. Gu, "Imaging by a high aperture optical system," J. Mol. Spectrosc. **40**, 1631–1651 (1993).